Electron-impact ionization cross-section measurements for U^{10+}, U^{13+}, and U^{16+}

D. C. Gregory, M. S. Huq,* and F. W. Meyer
Physics Division, Oak Ridge National Laboratory, Oak Ridge, Tennessee 37831-6372

D. R. Swenson†
Joint Institute for Laboratory Astrophysics, Boulder, Colorado 80309-0440
and Oak Ridge National Laboratory, Oak Ridge, Tennessee 37831-6372

M. Sataka
Department of Physics, Japan Atomic Energy Research Institute, Tokai-mura, Ibaraki, 319-11, Japan

S. Chantrenne
Lawrence Livermore National Laboratory, L-401, Livermore, California 94550
(Received 21 August 1989)

Absolute measurements are presented for electron-impact single ionization of U^{10+}, U^{13+}, and U^{16+}, and for double ionization of U^{10+} and U^{13+} from below the thresholds to 1500 eV. Metastable components are observed in all three incident-ion beams. The single-ionization cross sections are enhanced due to indirect ionization processes by factors of 4–20 near their peaks, and the double-ionization cross sections are apparently also dominated by indirect ionization. Good agreement is found with distorted-wave calculations for total ionization of U^{16+}, the only case where detailed calculations are available for comparison. Individual or closely spaced resonances are clearly resolved in the single-ionization channels for U^{13+} and U^{16+}.

INTRODUCTION

Uranium is the heaviest naturally occurring element and provides an extreme test for the application of relativistic atomic theory. It is not a particularly convenient element to work with, however, since access to pure uranium is somewhat restricted due to national security considerations. A number of compounds that form in discharges containing uranium are highly corrosive, and there are health hazards that are associated with any of the heavy metals. It is not surprising in light of these potential problems that very little work has been reported involving inelastic electron-impact collisions with uranium. Ionization of neutral uranium was reported by Halle, Lo, and Fite,[1] and a channeling experiment by Claytor *et al.*[2] yielded ionization cross sections for uranium ions in initial charge states 88+ through 91+ at an equivalent of 220 keV electron energy. Published theoretical work appears to be even more scarce, with one reported study of ionization of neutral uranium at relativistic energies by Scofield.[3]

A number of recent studies have dealt with other heavy elements. For example, giant shape resonances were predicted for several heavy atoms and ions (up to three times charged) by Younger[4] in 1987. While searching for these giant shape resonances in heavy ions, Müller and coworkers[5] first observed the resonant-excitation–double-autoionization (REDA) process. The complex electron structure of few-times-ionized heavy elements makes detailed analysis of such data difficult, but there are also numerous strong excitation channels that can potentially create a rich variety of easily observable indirect ionization effects. Uranium was chosen for the present study due to its potential for revealing new indirect ionization channels or enhanced examples of known effects.

One problem in interpreting data from ions of heavy elements involves the rearrangement of electrons as the charge increases. The ground electron configuration of atomic uranium, for instance, is $5f^3 6d 7s^2$, with three unfilled shells. U^{10+}, however, is truly isoelectronic with the Pb ground configuration ($6s^2 6p^2$). Unlike the neutral sequence from Pb to Os, electrons are removed from uranium ions from charge 10+ and 16+ without leaving multiple open subshells, so that $U^{16+}(5d^8)$ is not truly isoelectronic with $Os(5d^6 6s^2)$. It is not always obvious which excited configuration of an ion will have the lowest energy, and this also makes the prediction of metastable configurations more difficult. Table I presents a number of configuration-average energy levels for uranium ions of interest in the work presented here. These energies were calculated using the relativistic Hartree-Fock (HFR) code developed by Cowan.[6] Some of the configurations listed involve numerous levels spread over up to 80 eV, according to more detailed energy-level calculations which have been carried out for selected configurations.[7]

The first section briefly describes the experimental arrangement. A presentation and discussion of the single-ionization cross-section measurements follows, and Sec. III presents double-ionization results. Section IV discusses the observation of resonances in the single-ionization channel, and conclusions are presented in Sec. V.

I. EXPERIMENTAL ARRANGEMENT

The measurements utilized the Oak Ridge National Laboratory Electron Cyclotron Resonance (ORNL-ECR) ion source and the crossed electron-ion beams apparatus. Both have been described in detail previously,[8,9] so only a brief discussion will be given here. Uncertainties listed in the tables and shown in the figures are relative only, equivalent to one standard deviation (1 s.d.) for statistical uncertainties. The relative uncertainties are dominated by counting statistics, but also include other factors (such as variations in beam profile measurements and form-factor calculations) which differ between measurements. Absolute uncertainties are dominated by the relative contributions, but include other factors which all measurements of a given reaction have in common (transmission of signal ions to the detector, detector and electronics efficiencies, particle velocities, and current measurements). Absolute uncertainties for these measurements range from 8% to 10% for typical points near the peak of the cross-section curves, at an equivalent of 2 s.d. for statistical uncertainties.

TABLE I. Selected energy levels for uranium ions. Configuration-average calculations were performed with Cowan's HFR code (Ref. 6).

Ion	Configuration	Energy (eV)	Above ground (eV)
U^{10+}	$5p^6 5d^{10} 6s^2 6p^2$	0	0
	$6s^2 6p 6d$	37.4	37.4
	$5d^9 6s^2 6p^3$	99.2	99.2
	$5p^5 5d^{10} 6s^2 6p^3$	223.8	223.8
	$5s 5p^6 5d^{10} 6s^2 6p^3$	330.3	330.3
	$4f^{13} 5s^2 5p^6 5d^{10} 6s^2 6p^3$	390.9	390.9
U^{11+}	$5p^6 5d^{10} 6s^2 6p$	149.7	0
	$5d^9 6s^2 6p^2$	251.7	102.0
	$5p^5 5d^{10} 6s^2 6p^2$	376.5	226.8
	$5s 5p^6 5d^{10} 6s^2 6p^2$	483.1	333.4
	$4f^{13} 5s^2 5p^6 5d^{10} 6s^2 6p^2$	544.5	394.8
U^{12+}	$5p^6 5d^{10} 6s^2$	314.4	0
	$5d^8 6s^2 6p^2$	419.3	104.9
	$4f^{13} 5s^2 5p^6 5d^{10} 6s^2 6p$	713.2	398.8
U^{13+}	$5p^6 5d^{10} 6s$	524.9	0
	$5d^9 6s 6p$	634.5	109.6
	$5p^5 5d^{10} 6s^2$	727.6	202.7
	$5s 5p^6 5d^{10} 6s^2$	834.6	309.7
	$4f^{13} 5s^2 5p^6 5d^{10} 6s 6d$	930.1	405.2
U^{14+}	$5p^6 5d^{10}$	753.5	0
	$5p^5 5d^{10} 6s$	958.6	205.1
	$4f^{13} 5s^2 5p^{10} 6s$	1129.7	376.2
	$4d^9 4f^{14} 5s^2 5p^6 5d^{10} 6s$	1505.6	752.1
U^{15+}	$5p^6 5d^9$	1081.9	0
	$4f^{13} 5s^2 5p^6 5d^{10}$	1380.5	298.6
U^{16+}	$5p^6 5d^8$	1436.4	0
	$5p^6 5d^7 6s$	1526.4	90.0
	$4f^{13} 5s^2 5p^6 5d^9$	1739.9	303.5
U^{17+}	$5p^6 5d^7$	1817.6	0
	$5p^5 5d^8$	1944.6	126.9
	$5s 5p^5 5d^8$	2054.0	236.4
	$4f^{13} 5s^2 5p^5 5d^8$	2126.2	308.6
	$4d^9 4f^{14} 5s^2 5p^6 5d^8$	2501.7	684.1
U^{18+}	$5p^6 5d^6$	2226.1	0

The ion beams used in these measurements were produced in the ECR ion source from depleted UF_6 (i.e., predominantly U^{238}) obtained from the isotope separation operation in Oak Ridge. Although UF_6 is solid at room temperature, the vapor pressure was found to be adequate for use in the source without heating the sample. No mixing gas was used for these measurements. The charge-state distribution for optimized beams extracted from the source peaks at about U^{21+} when a uranium foil is used as the source of raw material, but the distribution shifts several charge states lower when using the UF_6. All of the ions in this study were at the peak or on the low side of the optimized charge-state distribution. As might be expected when operating under these conditions, all three ion beams in the present study show evidence of metastable components in the extracted beams. Typical beam currents transported through the apparatus and measured downstream of the collision volume averaged 50 electrical-nA (ion charge times particle flux) (with up to 100 nA maximum) for all three of the ions in this study. Overlaps with the unavoidable impurity ions OH^+ and O^+ made it impossible to extract clean beams of U^{14+} and U^{15+}, respectively. Limitations in our UF_6 supply and available beam time prevented our pursuing measurements involving U^{11+} and U^{12+}.

In a typical experiment, ion beams from the ECR source are transported through a beam line containing optics and differential pumping to the high-vacuum chamber shown in Fig. 1. In this chamber, the incident beam passes through one-dimensional einzel lenses and steering before entering the electrostatic analyzer marked "charge purifier" in the figure. Any ions that have changed charge due to collisions with background gas or grazing collisions with slits are removed by this analyzer. After passing through the collision region, which is located in the center of the electron gun, the ions enter a double-focusing magnetic analyzer which separates the unchanged ion beam from those ions which changed charge. The signal ions, with the same velocity as the incident beam but a higher charge, are focused onto the channel-electron multiplier labeled "ionized ion detector" in the figure. These ions are detected 90° out of the scattering plane in order to reduce the background caused by stray particles and photons. The detection efficiency for ions of this velocity is near 100%, and the sensitivity of the electronics is monitored by periodic pulse-height distribution measurements. The unchanged incident ion beam is captured in one of two movable cups, depending on the ratio of the incident-to-signal ion charge ratio. The apparatus, as shown in this figure, is capable of detecting ionization events with incident-to-signal ion charge ratios ranging from about $\frac{4}{5}$ to $\frac{16}{17}$. Additional lenses and cups shown in the ion flight path are used for beam tuning and diagnostic tests to ensure that all of the signal ions are incident on the multiplier. The

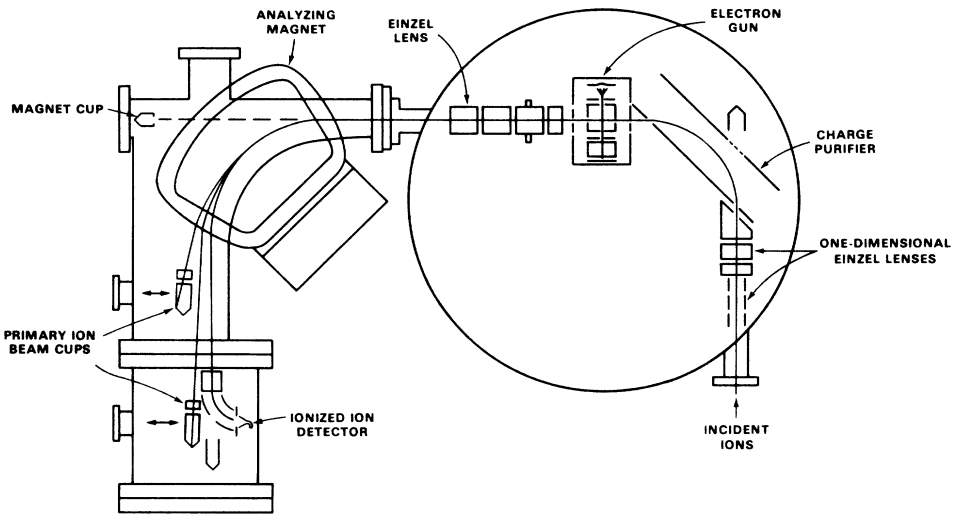

FIG. 1. ORNL crossed electron-ion beams interaction and charge analysis apparatus.

absolute ion beam current and accelerating voltage are carefully monitored.

The electron gun, located near the top of the central chamber in Fig. 1, is almost identical to the one described by Taylor *et al.*[10] The electron beam is confined by an axial magnetic field, and crosses the ion beam at 90°. The electron current is collected in an array of edge-on "razor blades" designed to minimize backscattering and secondary electron emission. The electron velocity in the collision region is derived from the accelerating voltage, including corrections for contact potentials and the beam space charge based on previous calibrations.[8,10] The uncertainty in the quoted collision energy ranges from ±0.2 eV at the lower energies to ±1 eV at 1500 eV. The energy spread in the electron beam is estimated to be between 1 and 2.5 eV over this energy range. A probe located at the crossing volume can be rotated to measure the spatial profile of either the electron or ion beam. The form factor, taking into account the overlap of the two beams, is calculated from these profiles. The absolute cross section σ at each energy E is determined by the signal count rate R, beam currents (I_i and I_e) and velocities (v_i and v_e), form factor F, and signal-particle counting efficiency D through the equation

$$\sigma(E)=\frac{Re^2v_iv_eF}{I_iI_e(v_i^2+v_e^2)^{1/2}D} . \quad (1)$$

II. SINGLE-IONIZATION CROSS-SECTION MEASUREMENTS

Cross-section measurements for single ionization of U^{10+}, U^{13+}, and U^{16+} are plotted in Figs. 2, 3, and 4 and listed in Table II. The relative uncertainties listed in Table II are equivalent to 1 s.d. for statistics. The relative uncertainties are smaller than the plotted points in each of the figures except for those few points where error bars are shown. The solid curves in Figs. 2 and 3 represent direct ionization from the ground configurations of $U^{10+}(5d^{10}6s^26p^2)$ and $U^{13+}(5p^65d^{10}6s)$, based on the semiempirical Lotz[11] formula. Configuration-average energies for ionization from appropriate subshells were calculated using Cowan's HFR code.[6] For U^{16+} in Fig. 4, the dashed curve is the Lotz estimate for direct ionization from the metastable $(4f^{14}5s^25p^65d^76s)$ configuration, and the solid curve is a distorted-wave calculation of total ionization (including excitation-autoionization effects) by Pindzola and Buie.[12]

The single-ionization cross-section curves presented here all contain the signature of metastable ions in the incident beams—the onset of ionization is observed in all

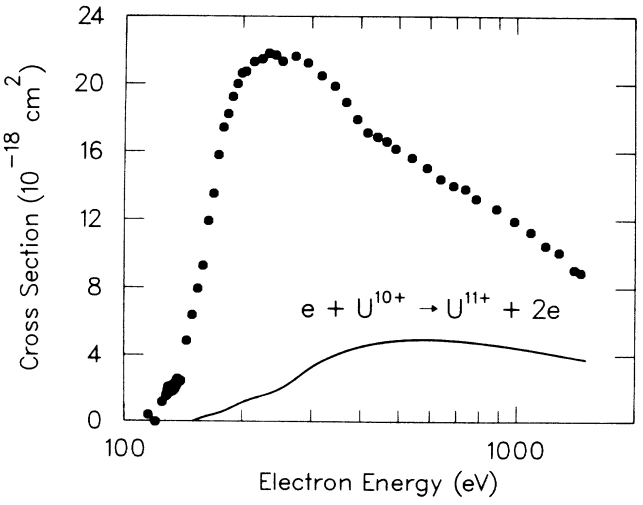

FIG. 2. Single-ionization cross sections for U^{10+}. Relative uncertainties at the 1 s.d. level are smaller than the plotted points. The solid curve is a Lotz calculation (Ref. 11) for direct ionization of ground-configuration $5d^{10}6s^26p^2$ electrons.

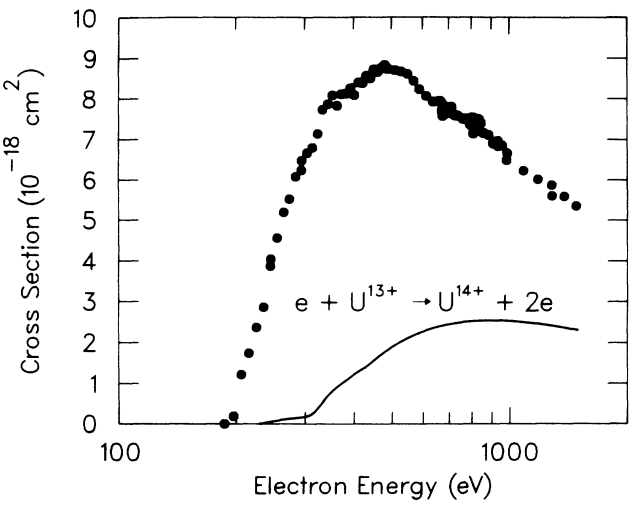

FIG. 3. Cross sections for single ionization of U^{13+}. Relative uncertainties at the 1 s.d. level are smaller than the plotted points. The solid curve is a Lotz calculation (Ref. 11) for direct ionization of ground configuration $5p^6 5d^{10} 6s$ electrons.

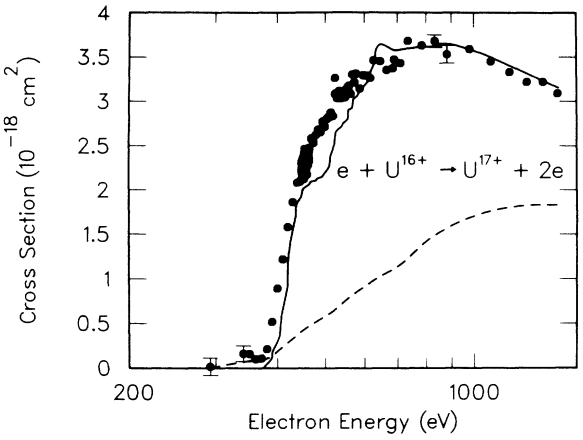

FIG. 4. Cross sections for single ionization of U^{16+}. Relative uncertainties are shown at the 1 s.d. level where larger than the plotted points. The dashed curve is a Lotz calculation (Ref. 11) for direct ionization of electrons in the $4f^{14}5s^2 5p^6 5d^7 6s$ (metastable) configuration. The solid curve is a distorted-wave calculation including excitation-autoionization effects (from Pindzola and Buie, Ref. 12).

TABLE II. Single-ionization cross sections for uranium ions. Cross-section uncertainties are relative only at the equivalent of 1 s.d. for statistics; collision energy uncertainties range from ±0.2 (at low energies) to ±1 eV (at high energies).

Collision energy (eV)	U^{10+} Cross section (10^{-18} cm^2)	Collision energy (eV)	U^{10+} Cross section (10^{-18} cm^2)
115.4	0.38±0.16	203.5	20.72±0.11
120.3	−0.04±0.16	213.3	21.29±0.16
125.3	1.14±0.19	223.9	21.46±0.16
128.4	1.51±0.17	233.0	21.79±0.13
129.4	1.72±0.17	242.6	21.69±0.13
130.0	2.06±0.15	252.4	21.32±0.13
130.5	1.91±0.16	272.3	21.62±0.12
131.4	1.86±0.16	292.5	21.22±0.09
132.5	1.84±0.14	317.5	20.47±0.18
133.3	1.84±0.14	343.4	19.85±0.12
134.4	1.92±0.14	367.0	18.88±0.11
135.0	2.17±0.20	392.0	17.89±0.11
135.4	2.15±0.16	416.0	17.10±0.18
136.2	2.30±0.13	440.7	16.85±0.11
137.2	2.56±0.16	465.0	16.58±0.12
138.2	2.40±0.21	489.9	16.15±0.05
139.8	2.44±0.15	539.3	15.63±0.12
144.8	4.85±0.11	588.4	15.05±0.13
149.5	6.40±0.21	637.4	14.39±0.12
154.5	7.95±0.15	687.4	13.99±0.05
159.4	9.30±0.23	735.8	13.81±0.07
164.3	11.90±0.15	784.9	13.23±0.08
169.2	13.52±0.17	883.1	12.66±0.08
174.2	15.79±0.09	981.9	11.91±0.05
179.1	17.40±0.13	1080	11.27±0.05
183.9	18.20±0.11	1179	10.48±0.08
188.7	19.20±0.28	1276	10.09±0.05
193.9	19.98±0.13	1396	9.08±0.04
198.7	20.62±0.15	1451	8.91±0.06

TABLE II. (*Continued*).

Collision energy (eV)	U^{13+} Cross section (10^{-18} cm^2)
186.8	0.00±0.10
197.0	0.19±0.13
206.2	1.22±0.11
215.9	1.74±0.08
226.0	2.37±0.09
235.6	2.86±0.08
245.3	3.87±0.07
245.7	4.04±0.11
255.1	4.55±0.06
264.9	5.18±0.05
274.6	5.51±0.06
284.6	6.07±0.05
294.4	6.23±0.05
294.7	6.47±0.10
304.1	6.66±0.05
313.9	6.79±0.07
323.9	7.13±0.07
333.5	7.72±0.07
343.9	7.86±0.09
353.2	8.08±0.07
363.1	7.82±0.08
372.6	8.11±0.07
382.3	8.12±0.08
392.6	8.26±0.06
401.9	8.08±0.08
411.8	8.40±0.07
421.6	8.38±0.07
431.3	8.56±0.08
441.6	8.50±0.07
450.8	8.72±0.08
461.1	8.66±0.08
470.7	8.75±0.08
480.6	8.83±0.08
491.0	8.73±0.13
510.0	8.70±0.06
529.0	8.67±0.08
549.4	8.61±0.06
569.1	8.44±0.05
588.6	8.23±0.05
613.1	8.06±0.06
637.8	7.92±0.06
662.5	7.94±0.06
667.1	7.93±0.05
672.0	7.68±0.05
673.9	7.58±0.04
676.9	7.84±0.05
687.0	7.65±0.04
698.6	7.66±0.04
711.3	7.80±0.06
723.4	7.59±0.04
736.1	7.58±0.05
760.8	7.50±0.04
785.4	7.50±0.06
794.6	7.38±0.03
804.8	7.53±0.05
807.6	7.14±0.03
809.6	7.16±0.03
814.8	7.49±0.05
824.4	7.46±0.05
834.3	7.49±0.07
844.1	7.40±0.04
859.0	7.15±0.04
883.5	7.11±0.05
907.9	6.90±0.04
932.6	6.96±0.05
935.8	6.83±0.05
957.3	6.85±0.03
982.0	6.48±0.04
985.3	6.66±0.05
1084	6.23±0.04
1182	6.01±0.03
1281	5.87±0.04
1281	5.59±0.04
1379	5.58±0.03
1478	5.34±0.03

Collision energy (eV)	U^{16+} Cross section (10^{-18} cm^2)
292.2	0.02±0.10
341.1	0.16±0.09
351.4	0.16±0.08
361.3	0.10±0.08
371.1	0.11±0.08
380.8	0.21±0.09
390.2	0.52±0.06
399.7	0.89±0.08
410.1	1.22±0.06
419.8	1.58±0.08
429.7	1.86±0.09
439.4	2.08±0.06
444.3	2.09±0.07
449.2	2.31±0.08
453.8	2.35±0.08
458.6	2.17±0.07
464.3	2.47±0.05
469.1	2.58±0.03
474.3	2.53±0.04
478.9	2.62±0.04
484.1	2.68±0.03
489.2	2.65±0.03
494.0	2.77±0.03
498.9	2.71±0.03
503.7	2.80±0.06
508.7	2.82±0.06
513.5	2.87±0.04
518.3	2.83±0.04
523.2	3.20±0.03
528.3	3.03±0.03
533.1	3.11±0.03

TABLE II. (*Continued*).

Collision energy (eV)	U^{16+} Cross section (10^{-18} cm^2)	Collision energy (eV)	U^{16+} Cross section (10^{-18} cm^2)
538.1	3.03±0.05	646.1	3.45±0.05
543.0	3.04±0.06	665.8	3.35±0.07
548.0	3.04±0.06	688.2	3.45±0.03
552.7	3.14±0.04	709.9	3.43±0.05
557.7	3.17±0.04	734.5	3.68±0.08
562.5	3.08±0.03	783.8	3.63±0.07
567.6	3.30±0.03	832.5	3.68±0.07
572.3	3.21±0.04	881.7	3.53±0.10
577.4	3.31±0.03	979.7	3.59±0.06
587.4	3.14±0.06	1082	3.45±0.05
597.0	3.29±0.05	1180	3.33±0.06
606.8	3.29±0.05	1279	3.22±0.05
616.6	3.26±0.05	1378	3.22±0.04
626.4	3.46±0.06	1476	3.09±0.05

three cases at energies lower than expected for ground-configuration ions. In U^{10+}, the observed ionization threshold, at about 122 eV, is consistent with that predicted for a number of excited configurations, including $6s^2 6p\,6d$. The average energy for ionization of the ground configuration ($6s^2 6p^2$) is 30 eV higher. Similarly, the observed threshold for ionization of U^{13+} is near 200 eV (versus 227 eV for the ground $5d^{10}6s$ configuration) and the threshold for U^{16+} is found near 300 eV (versus 381 eV for the ground $5d^8$ configuration). The observed ionization onsets for these two ions are consistent with those expected for, e.g., U^{13+} in the $5d^{10}6p$ configuration and U^{16+} in the $5d^7 6s$ configuration.

The cross-section curves for both U^{10+} and U^{13+} rise steeply from the observed thresholds, indicating significant excitation-autoionization contributions even below the ground-configuration ionization threshold energy. A slight change in slope is observed at the ground-configuration thresholds as new direct and indirect ionization channels open. Comparing the two measurements to the Lotz cross-section predictions, it is clear that indirect ionization dominates over the entire energy range studied here. No sharp features are observed which would indicate a single especially strong excitation onset in either curve. Rather, the indirect portion of the ionization cross section is made up of many small incremental contributions due to excitation-autoionization and (probably) resonant-excitation–double-autoionization processes that result in the observed smooth curve. The rather sharp drop in cross section between 300 and 400 eV for U^{10+} is similar to features which have been observed in other systems[13] (e.g., Xe^{3+}). This energy dependence is consistent with that expected for a group of non-dipole-allowed excitations to autoionizing configurations. At higher energies, the slower falloff due to dipole-allowed excitations is seen to dominate. At much higher energies (e.g., above 5–10 keV), direct ionization is expected to dominate the total cross section. The energy dependence of the U^{13+} cross section is similar, except that no sharp drops in cross section are observed. Apparently, no energy region is dominated by non-dipole-allowed excitation-autoionization features.

The cross-section curve for ionization of U^{16+} is different from the two cases described above in some important respects. The ionization threshold is indicative of a metastable component in the incident-ion beam, but a sharp change in slope is observed at the ground-configuration ionization threshold, in contrast to the slight changes observed for the other two ions in this study. The dashed line in Fig. 4 is a Lotz apparent cross section for direct ionization of a 100% metastable ($5d^7 6s$) ion beam. The good agreement between the Lotz results and experiment between 300 and 400 eV indicates a large (near 100%) metastable fraction and little or no excitation-autoionization contribution below the $5d^7$ ionization onset. Above the ground-configuration threshold, a large indirect ionization contribution is observed, with no especially sharp features.

Accurate calculations for ionization of ground-configuration U^{16+} are available for comparison with the present measurements.[12] Direct ionization in the distorted-wave (DW) approximation is within a few percent of the Lotz prediction for this ion, so they are not plotted separately in Fig. 4. Direct ionization from the ground and metastable configurations are also essentially equal above 300 eV. The DW total ionization calculations explicitly included 69 transitions involving $4d$, $4f$, $5s$, and $5p$ electrons to autoionizing excited configurations up to $n = 10$, with an extrapolation procedure used to approximate the effects of transitions to higher levels. The agreement between the theory (solid line in Fig. 4) and experiment is impressive. It is thought that theory underestimates the measured cross section between 450 and 550 eV due to the effects of numerous REDA transitions in this energy range.

III. DOUBLE-IONIZATION CROSS SECTIONS

The data for double ionization of U^{10+} and U^{13+} are plotted in Figs. 5 and 6 and listed in Table III. A small but significant negative cross section is observed below threshold for U^{10+}; this phenomenon must be due to an

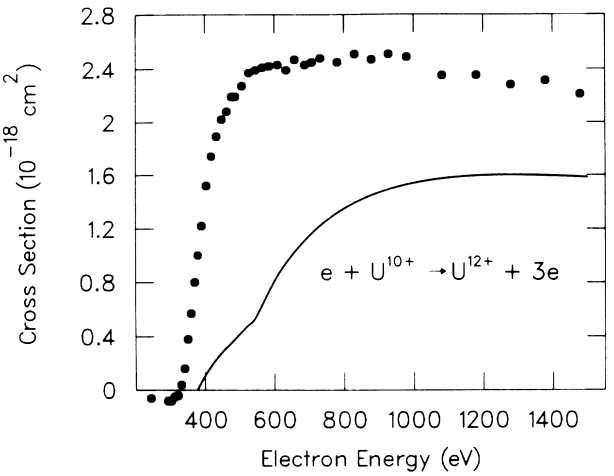

FIG. 5. Double-ionization cross sections for U^{10+}. Relative uncertainties at the 1 s.d. level are smaller than the plotted points. The solid curve is a Lotz calculation (Ref. 11) for direct single ionization of $4f^{14}5s^25p^6$ electrons, which should contribute to double ionization following autoionization.

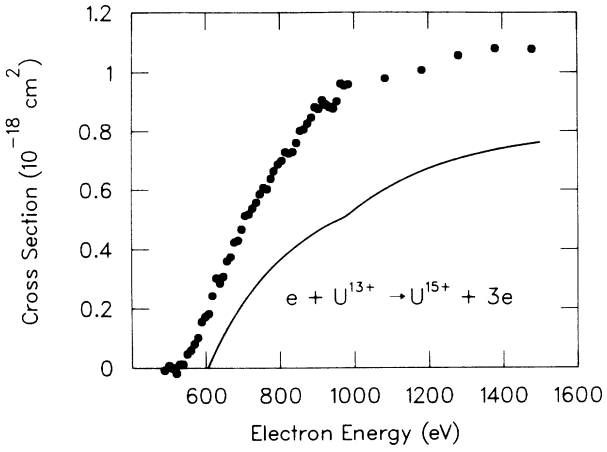

FIG. 6. Double-ionization cross sections for U^{13+}. Relative uncertainties at the 1 s.d. level are smaller than the plotted points. The solid curve is a Lotz calculation (Ref. 11) for direct single ionization of $4d^{10}4f^{14}$ electrons, which should contribute to double ionization following autoionization.

experimental problem (such as space-charge modulation) rather than physics. The effect is small and should decrease with increasing energy (assuming it is due to modulation), so it is not expected to affect the interpretation of the results. Considering the presence of a significant metastable fraction in the incident U^{10+} beam, we might expect the onset of double ionization as much as 30 eV below the 314-eV ground-configuration threshold. In fact, the cross section becomes significant at about 325 eV.

A very rough estimate of the direct double-ionization cross section may be obtained in the binary-encounter approximation (BEA) following the work of Gryzinski.[14] From the energy levels in Table I, we expect direct double ionization from the $5d$, $6s$, and $6p$ subshells of U^{10+}. The peak BEA direct double-ionization cross section is a factor of 100 smaller than the observed peak value, and occurs near 1500 eV rather than near threshold. Clearly, the double-ionization cross section is dominated by indirect processes such as ionization-autoionization and excitation–double-ionization. The solid curve in Fig. 5 is a Lotz calculation for direct single ionization from the $4f$, $5s$, and $5p$ subshells of U^{10+}. This is the predicted contribution due to ionization autoionization, and it accounts for approximately half of the observed cross section. The rather steep onset of ionization near threshold is indicative of an excitation process which leaves the ion in a configuration which stabilizes to produce a net double-ionization event. This part of the cross section is probably dominated by excitation of $4f$ electrons, but there are currently no excitation calculations available for use in estimating the contribution.

The threshold for double ionization of U^{13+} is observed near 550 eV, the expected direct double-ionization threshold for ground-configuration U^{13+}. As was the case for U^{10+}, the presence of a metastable component in the incident beam does not significantly affect the cross section for double ionization. The BEA calculation of direct double ionization from the $5d$ subshell again predicts a peak cross section a factor of 100 smaller than that observed. The solid curve in Fig. 6 is a Lotz calculation for direct single ionization of the $4d$ ad $4f$ subshells, which should contribute to this cross section following autoionization. The $4d$ contribution may be split between net double and triple ionization, but the full cross section is assumed in this calculation. As was the case for U^{10+} double ionization, the remaining cross section is assumed to be the result of excitation followed by double autoionization. Excitations involving the $4d$ subshell probably dominate.

Both double-ionization cross-section measurements are strongly dominated by indirect single-electron processes, with (estimated) roughly equal contributions from ionization-autoionization and excitation–double-autoionization processes. In both cases, the peak double-ionization cross sections are about a factor of 10 smaller than the corresponding single-ionization cross sections. A detailed analysis of the cross section curves must await excitation and branching calculations.

The fact that the presence of metastable ions in the incident beams does not affect the thresholds for double ionization of these two ions is at first surprising. However, we should note that the contributions of direct double ionization are negligible in both cases, so that the effect of the metastable ions on indirect ionization is the important consideration. The thresholds for excitation or single ionization of electrons in inner subshells is not significantly affected by moving one electron between two outer subshells. Thus the threshold and magnitude of multiple ionization resulting from excitation-autoionization or ionization-autoionization processes should not be affected by the presence of metastable ions unless the relatively small added energy opens additional channels which would not contribute in the case of

ground-configuration targets. The observed onset of significant multiple ionization does not always coincide with the lowest energy required for multiple ionization, but more usually begins at the onset of the lowest-energy single-electron excitation or ionization transition which will contribute to the multiple-ionization channel.

IV. RESONANT-EXCITATION–DOUBLE-AUTOIONIZATION PROCESS

One of the purposes of this project was to investigate the role of resonant processes in ionization of highly charged heavy ions. The resonant process that has been

TABLE III. Double-ionization cross sections for U^{10+} and U^{13+}. Uncertainties are as described for Table II. Note that the cross section is in different units than in Table II.

U^{10+}		U^{13+}	
Collision energy (eV)	Cross section (10^{-19} cm^2)	Collision energy (eV)	Cross section (10^{-19} cm^2)
243.5	−0.61±0.22	549.7	0.47±0.14
292.3	−0.84±0.19	559.6	0.60±0.16
302.1	−0.79±0.19	569.3	0.81±0.11
311.9	−0.53±0.20	579.1	1.03±0.16
321.7	−0.38±0.19	589.1	1.56±0.14
331.4	0.42±0.18	598.7	1.73±0.14
341.2	1.61±0.21	608.7	1.83±0.18
350.7	3.82±0.17	618.5	2.43±0.14
360.7	5.68±0.16	628.4	3.03±0.14
370.4	7.98±0.16	638.3	2.85±0.22
380.1	9.95±0.16	648.3	3.08±0.20
389.9	12.22±0.18	658.1	3.60±0.12
404.3	15.23±0.17	667.9	3.74±0.17
419.0	17.36±0.19	677.9	4.24±0.13
433.7	18.94±0.25	688.3	4.30±0.04
448.2	20.18±0.27	697.5	4.67±0.13
463.2	20.84±0.26	707.3	5.15±0.13
477.6	21.92±0.28	717.3	5.17±0.13
487.6	21.91±0.21	727.0	5.36±0.15
507.1	22.67±0.24	736.8	5.56±0.14
526.7	23.73±0.26	746.9	5.85±0.11
546.3	23.94±0.45	756.7	6.07±0.11
565.9	24.08±0.22	766.7	6.02±0.11
585.2	24.17±0.24	776.5	6.37±0.11
609.6	24.32±0.28	784.4	6.63±0.08
634.2	23.88±0.24	795.9	6.86±0.11
658.7	24.71±0.22	805.7	6.98±0.14
687.6	24.28±0.09	815.6	7.28±0.17
707.5	24.46±0.21	825.5	7.23±0.11
732.2	24.83±0.21	835.5	7.28±0.13
781.4	24.52±0.25	845.5	7.59±0.16
830.2	25.07±0.22	855.4	8.01±0.15
879.1	24.67±0.28	865.3	8.05±0.13
928.0	25.11±0.21	875.0	8.26±0.13
980.5	24.88±0.19	885.6	8.46±0.10
1082	23.49±0.19	894.8	8.81±0.14
1180	23.45±0.18	904.8	8.75±0.13
1279	22.84±0.19	914.7	9.05±0.13
1378	23.10±0.20	924.4	8.90±0.13
1478	22.14±0.15	934.3	8.81±0.12
		944.3	8.76±0.12
U^{13+}		954.2	9.01±0.15
Collision energy (eV)	Cross section (10^{-19} cm^2)	964.1	9.61±0.22
		974.0	9.54±0.13
487.8	−0.08±0.15	984.5	9.58±0.12
500.6	0.08±0.13	1083	9.79±0.13
510.4	−0.00±0.14	1182	10.07±0.12
520.2	−0.18±0.12	1281	10.57±0.09
530.1	0.13±0.15	1380	10.81±0.10
538.4	0.13±0.09	1479	10.78±0.08

most extensively discussed in connection with ionization involves two steps. First, the projectile electron excites an inner target electron while being captured into an excited level of the target ion. Such a doubly (or more) excited ion may eject a single electron (resulting in a resonance in the elastic scattering cross section and no net change in ion charge), radiatively stabilize (dielectronic recombination, resulting in a net reduction in ion charge), or eject two electrons, which is called the resonant-excitation–double-autoionization process and results in a net ionization event.[15] If many such resonances overlap, a smooth enhancement of the cross section may be observed (see, e.g., Xe^{3+} in Ref. 16 and U^{16+} in this paper). The signature of an isolated, single REDA event is a sharp resonance feature on top of the smooth total ionization cross-section curve.

The data in Figs. 3 and 4 for U^{13+} and U^{16+} include some energy regions where cross-section measurements only a few eV apart differ by significantly more than their combined relative uncertainties. This is an indication of a contribution to the cross section due to a process with a sharp energy dependence, and the energy regions of interest were investigated more carefully. In two cases, one each for U^{13+} and U^{16+}, resonance features were isolated. The measurements are shown in Figs. 7 and 8, with relative uncertainties. For U^{13+}, the data shown were collected in two sets, indicated by the circles and squares. For U^{16+}, the three lowest-energy and two highest-energy points were measured independent of the remaining single data set. Each of the resonance scans is actually the accumulated result of hundreds of scans over the appropriate energy range, with a dwell time of approximately 4 s per data point per scan. This procedure helps cancel any drifts or instabilities with periods longer than about a minute.

The resolution of the observed features may be limited by either the energy resolution of the electron beam or by the presence of a number of overlapping resonances. The best-resolved feature observed here is the lowest-energy "peak" in Fig. 7 (for U^{13+}). The resolution of the electron beam [full width at half maximum (FWHM)] at that

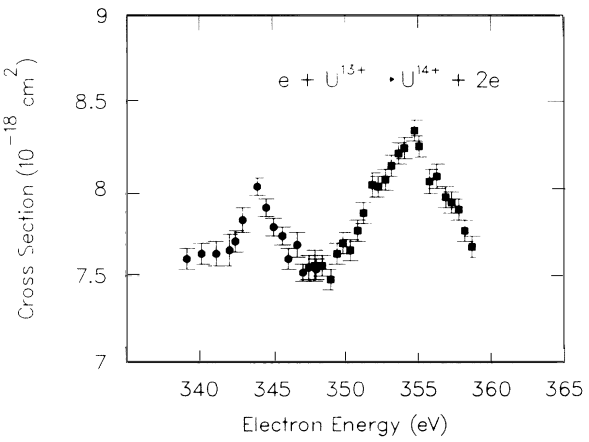

FIG. 7. Resonance structures in the single-ionization cross section of U^{13+}.

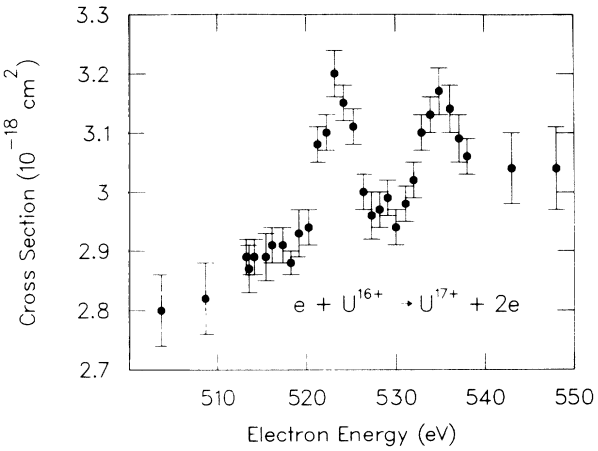

FIG. 8. Resonance structures in the single-ionization cross section of U^{16+}.

energy is expected to be just over 2 eV, approximately the same as that observed for this feature. Thus, either the feature is made up of several resonances which occur at almost exactly the same energy, or there is a single resonance which adds 0.4×10^{-18} cm^2 to the cross section with 2-eV resolution. The coincidence of numerous isolated resonances falling at the same energy seems unlikely, and we speculate that there may be some very strong single resonances in highly charged heavy ions. The other feature in the U^{13+} scan is about 5 eV wide and clearly is made up of two or more overlapping resonances. Similarly, the two features in the U^{16+} scan are probably made up of overlapping resonances. A preliminary analysis[17] of the transitions which could contribute to these resonance features indicates that, for U^{13+}, the $U^{12+}[4f_{7/2}]6s6d_{5/2}6f_{7/2}$ is the likely intermediate recombined level. A similar study has not been made for U^{16+}.

V. CONCLUSIONS

Cross-section measurements have been presented for single ionization of U^{10+}, U^{13+}, and U^{16+} and for double ionization of U^{10+} and U^{13+}. Metastable ions are present in all three incident beams, although the cross-section measurements for double ionization and for single ionization of U^{16+} are not significantly influenced by the metastable ions. Indirect processes dominate all of the cross-section curves, and good agreement is found with distorted-wave calculations for U^{16+} which include the effects of excitation autoionization. Peak cross sections for double ionization are found to be about 10% of the corresponding peak single-ionization values. Resonant ionization features which apparently are made up of single or a few large overlapping resonances have been measured for single ionization of U^{13+} and U^{16+}. Additional detailed calculations will be necessary in order to fully understand the results, but interpretations based on available information indicate that the physics of these systems is similar to that observed in other heavy ions such as those of the xenon isonuclear sequence.

ACKNOWLEDGMENTS

We gratefully acknowledge helpful discussions with R. A. Phaneuf and C. Bottcher, the use of unpublished work by S. M. Younger and M. Chen, and technical assistance from J. W. Hale. M. S. Huq received support through a Postgraduate Research Training Program, administered by Oak Ridge Associated Universities (ORAU) for the U.S. Department of Energy. This research was supported in part by the Office of Fusion Energy, U.S. Department of Energy, under contract No. DE-AC05-84OR21400 with Martin Marietta Energy Systems, Inc.

---

*Present address: Yale University School of Medicine, Hunter Radiation Therapy 215, New Haven, CT 06511-8040.

†Present address: Los Alamos National Laboratory, MP-5, H838, Los Alamos, NM 87545.

[1]J. C. Halle, H. H. Lo, and W. L. Fite, Phys. Rev. A **23**, 1708 (1981).

[2]Nelson Claytor, B. Feinberg, Harvey Gould, Curtis E. Bemis, Jr., Jorge Gomez del Campo, Carl A. Ludemann, and Charles A. Vane, Phys. Rev. Lett. **61**, 2081 (1988).

[3]J. H. Scofield, Phys. Rev. A **18**, 963 (1978).

[4]Stephen M. Younger, Phys. Rev. A **35**, 2841 (1987).

[5]A. Müller, K. Tinschert, G. Hofmann, E. Salzborn, and G. H. Dunn, Phys. Rev. Lett. **61**, 70 (1988).

[6]R. D. Cowan, *The Theory of Atomic Structure and Spectra* (University of California Press, Berkeley, 1981); R. D. Cowan and D. C. Griffin, J. Opt. Soc. Am. **66**, 1010 (1976).

[7]S. M. Younger (unpublished).

[8]D. C. Gregory, L. J. Wang, F. W. Meyer, and K. Rinn, Phys. Rev. A **35**, 3256 (1987).

[9]F. W. Meyer, Nucl. Instrum. Methods Phys. Res. B **9**, 532 (1985).

[10]P. O. Taylor, K. T. Dolder, W. E. Kauppila, and G. H. Dunn, Rev. Sci. Instrum. **45**, 538 (1974).

[11]W. Lotz, Z. Phys. **216**, 241 (1968).

[12]M. S. Pindzola and M. J. Buie, Phys. Rev. A **39**, 1029 (1989).

[13]D. C. Gregory, P. F. Dittner, and D. H. Crandall, Phys. Rev. A **27**, 724 (1983).

[14]Michal Gryzinski, Phys. Rev. **138**, A336 (1965).

[15]The REDA process was first predicted to significantly influence total ionization cross sections by K. J. LaGattuta and Y. Hahn, Phys. Rev. A **24**, 2273 (1981).

[16]D. C. Griffin, C. Bottcher, M. S. Pindzola, S. M. Younger, D. C. Gregory, and D. H. Crandall, Phys. Rev. A **29**, 1729 (1984).

[17]Mau H. Chen (unpublished).